

Effect of doping on structural and optical properties of ZnO nanoparticles: study of antibacterial properties

P. MADDAHI^{1,2*}, N. SHAHTAHMASEBI^{1,2}, A. KOMPANY^{1,2}, M. MASHREGHI^{2,3},
S. SAFAEE^{1,2}, F. ROOZBAN¹

¹Department of Physics, Ferdowsi University of Mashhad, Mashhad, Iran

²Nanoresearch Center, Ferdowsi University of Mashhad, Mashhad, Iran

³Department of Biology, Ferdowsi University of Mashhad, Mashhad, Iran

Sol-gel method was successfully used for synthesis of ZnO nanoparticles doped with 10 % Mg or Cu. The structure, morphology and optical properties of the prepared nanoparticles were studied as a function of doping content. The synthesized ZnO:(Mg/Cu) samples were characterized using XRD, TEM, FTIR and UV-Vis spectroscopy techniques. The samples show hexagonal wurtzite structure, and the phase segregation takes place for Cu doping. Optical studies revealed that Mg doping increases the energy band gap while Cu incorporation results in decrease of the band gap. The antibacterial activities of the nanoparticles were tested against *Escherichia coli* (Gram negative bacteria) cultures. It was found that both pure and doped ZnO nanosuspensions show good antibacterial activity which increases with copper doping, and slightly decreases with adding Mg.

Keywords: ZnO nanoparticles; sol-gel; antibacterial; growth curve

© Wroclaw University of Technology.

1. Introduction

Zinc oxide having interesting physical and chemical properties, together with its cost-effective manufacturing process and abundance in nature, is a promising material for different applications, which has been intensively studied in past decades. The interest in ZnO is fueled and stimulated by its excellent properties such as wide direct band gap ($E_g \sim 3.36$ eV at 300 K), high exciton binding energy (60 meV), good piezoelectric characteristics, chemical stability, and biocompatibility which make it a good candidate for diverse application including light-emitting diodes, laser diodes, solar cells, optoelectronic switches, surface acoustic wave devices, hydrogen-storage devices, transparent electrodes, transparent thin-film transistors and sensors [1–5].

On the other hand, increasing concern about microbial contamination has led to the extensive use of antibacterial agents, especially inorganic metal

oxides such as MgO, CuO, TiO₂ and ZnO. Zinc oxide, as an inorganic antibacterial agent, has a key advantage due to its biocompatibility, antibacterial activity in neutral region (pH 7) even in darkness, non-toxicity to human, ability to withstand harsh condition, and being more durable, in comparison with the conventional organic materials [6], which makes it a good candidate for antibacterial applications from medical to industrial use. Although the exact mechanism of its antibacterial action is not clearly known, several mechanisms have been proposed: photocatalyst activities, electrostatic interactions [7], metal ion release, ROS (Reactive Oxygen Species) generation [8], membrane damage. Cellular internalization of the nanoparticles has also been reported [9]. Results of the antibacterial activity of ZnO nanostructures show that it increases with decreasing the particles size [8]. The crystallographic orientation has no effect [6], while increasing the lattice constant causes the increase of its antibacterial activity [10].

As particle size is reduced from micrometer to nanometer scale, the physical properties can

*E-mail: parisa_maddahi@yahoo.com

change dramatically. The enhanced bactericidal effectiveness of metal nanoparticles has been suggested to be due to their high surface-to-volume ratio. Such characteristics should allow them to interact closely with bacterial membranes, in addition to the release of metal ions. Therefore nanotechnology, by enabling the manipulation of the size and the shape of the particles, could have a dramatic influence on their antibacterial behavior [7]. Doping could also alter the bactericidal effect of ZnO as reported in the work by Yamamoto et al. [11].

One of the other advantages of ZnO is its color. Zinc oxide as a coating is colorless and transparent, and in the form of nanoparticles it is white; therefore it is a suitable choice in the applications where the appearance and aesthetic matter, such as orthodontic devices. This work is an attempt to enhance and optimize the antibacterial behavior of ZnO nanoparticles through doping. For this aim, nanoparticles of ZnO doped with Mg and Cu were synthesized via sol-gel method and the effects of the dopants on the structural and optical properties as well as antibacterial activity were studied.

2. Experimental methods

ZnO:Mg/Cu nanoparticles were synthesized by refluxing solution of $\text{Zn}(\text{NO}_3)_2 \cdot 6\text{H}_2\text{O}$ and magnesium chloride ($\text{MgCl}_2 \cdot 6\text{H}_2\text{O}$)/copper nitrate ($\text{Cu}(\text{NO}_3)_2 \cdot 3\text{H}_2\text{O}$) in a mixture of absolute ethanol and deionized water (1:1). Ethylene glycol and acetic acid were used as polymerization and complexing agents, respectively. The homogeneous mixture was maintained under reflux at 100 – 110 °C for 6 hours. After vaporizing the excess solvents, a white powder was obtained. Before characterization, the powders were first calcined at 450 °C and then milled.

To make nanofluid for antibacterial tests, certain amount of NPs was mixed with deionized water (1 g/L), and stirred vigorously. In order to obtain a homogenous nanofluid, a ball-mill mixer (Retsch MM400, 28 Hz, 5 min) was used. For sterilization, the prepared nanofluids were autoclaved at 121 °C and a pressure of 2 MPa for 20 min.

The typical XRD spectra of the prepared powders were characterized using X ray diffractome-

ter (Cu K_α line $\lambda = 0.15406$ nm) in the range of $20^\circ < 2\theta < 60^\circ$ and 0.04 degree step size.

The morphology and size of the samples were examined by TEM (Leo 912 AB) images.

Fourier transform infrared spectroscopy (FTIR) study was carried out for investigating the chemical composition of the samples, using FTIR spectrophotometer (Shimadzu 4300) in the range of 400 – 4000 cm^{-1} .

Antibacterial tests were performed by measuring the growth curve of *E. coli* HB 101 incubated in the LB broth medium in the presence of nanofluids [8]. The growth curves were obtained by measuring time evolution of optical density (OD) of the sample. The measurements were performed at 600 nm wavelength using UV/Vis spectrophotometer (WPA LightWave S2000) at a frequency of once in an hour.

3. Results and discussions

3.1. Structural studies

Fig. 1 shows the XRD patterns of the samples. The patterns show that ZnO particles possess polycrystalline hexagonal wurtzite structure. The patterns of ZnO:Cu nanoparticles reveal that although the ZnO peaks are more evident, two minor peaks assigned to CuO monoclinic phase are also observable, which verifies the existence of secondary phase. Literature data show that only samples with copper content lower than 15 % are one-phase wurtzite-like $\text{Cu}_x\text{Zn}_{1-x}\text{O}$, while those with higher copper content include a tenorite-like oxide ($\text{Zn}_x\text{Cu}_{1-x}\text{O}$) phase [12]. The change in the lattice parameters of the doped samples is negligible.

In the case of ZnO:Mg nanoparticles, no peaks originating from MgO rock-salt structure have been detected. This result indicates that Mg^{2+} can be incorporated into the ZnO lattice with no phase segregation taking place, which was not unexpected because Mg and Zn ionic radii are almost the same (0.57 Å for Mg and 0.60 Å for Zn) [13].

3.2. Morphological studies

TEM images of the pure ZnO and ZnO doped with 10 % of Mg and Cu are shown in Fig. 2. These

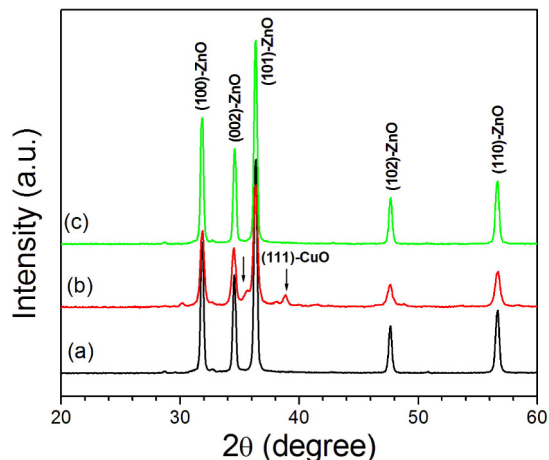
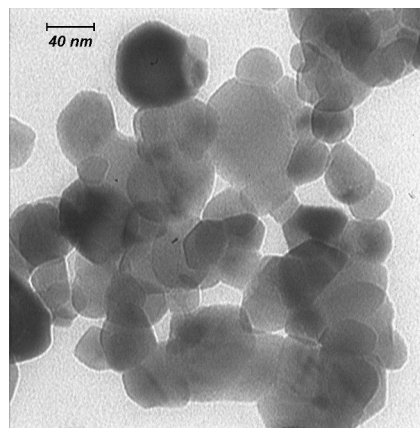


Fig. 1. XRD patterns of (a) pure ZnO, (b) ZnO:Cu and (c) ZnO:Mg nanoparticles.

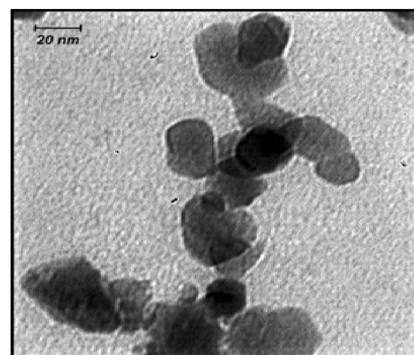
images verify the growth of nanoparticles with relatively uniform size distribution. The average size of pure ZnO samples is in the range of 30 – 44 nm, while in the image corresponding to Cu doped sample, the sizes of the particles are in 20 – 46 nm range. Mg doping results in the formation of larger particles of the order of 40 – 55 nm.

3.3. FTIR analysis

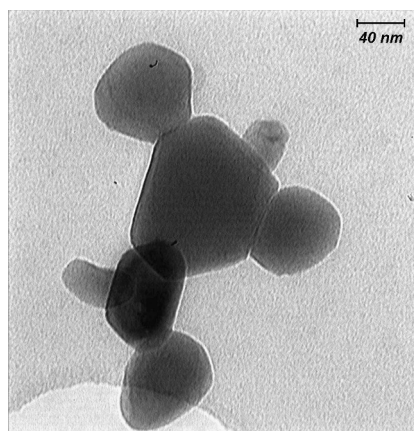
FTIR spectra of pure ZnO and doped ZnO nanoparticles are shown in Fig. 3. The high intensity absorption peaks from the vibration of hydroxyl group at $\sim 3400\text{ cm}^{-1}$ and $\sim 1600\text{ cm}^{-1}$ can be assigned to the O–H stretching vibrations due to the absorbed water on the surface of the samples. The absorption at $\sim 2360\text{ cm}^{-1}$ is because of the presence of CO_2 molecules in the environment [14]. As it can be seen in Fig. 3b, for the pure sample, the intense absorption peak at $\sim 435\text{ cm}^{-1}$ is related to the stretching vibrations of Zn–O bond. By Mg incorporation, an additional absorption peak at $\sim 520 - 535\text{ cm}^{-1}$ is observed. In the samples doped with copper, an absorption band near 620 cm^{-1} is also recognizable, which is related to vibration of Cu–O bond [15]. One can also observe the shifting of stretching bond position of Zn–O towards higher wave numbers, from 435 to 453 cm^{-1} , by a corresponding increase in Mg molar concentration from 0 to 0.1. This shift is attributed to substitution of Zn by lighter Mg



(a)



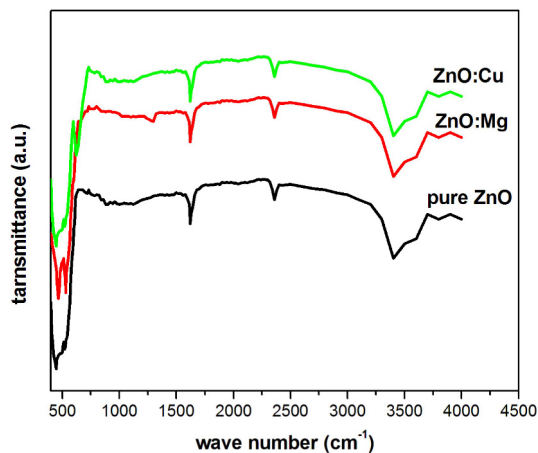
(b)



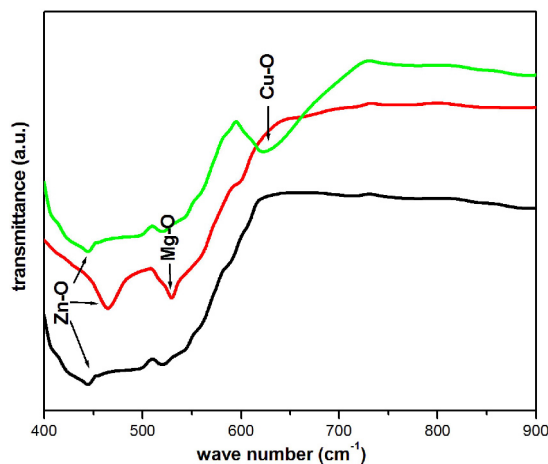
(c)

Fig. 2. TEM images of pure ZnO, ZnO:Cu and ZnO:Mg nanoparticles.

atoms [16]. This shift is not recognizable in Cu doped particles because Zn and Cu masses are rather similar (63.5 amu for Cu and 65.4 amu for Zn).



(a)



(b)

Fig. 3. (a) FTIR spectra of pure and doped ZnO samples, (b) the same FTIR spectra in the range of 400 – 900 cm^{-1} .

3.4. Optical studies

Fig. 4 shows the optical absorption spectra of the samples examined at room temperature. This figure shows that all samples have sharp absorption edges in the UV region. The observed absorption edge decreases from 363 to 355 nm with incorporation of Mg atoms while Cu doping results in absorption peak tending toward larger wavelengths.

The direct band gap of the samples was calculated using Tauc relation as follows:

$$\alpha h\nu = A(h\nu - E_g)^n \quad (1)$$

where α is the absorption coefficient, A is a con-

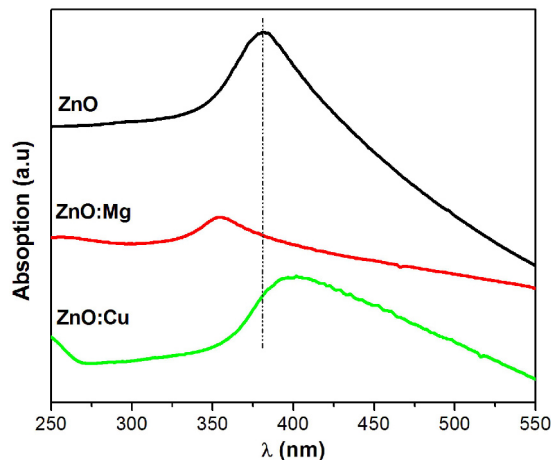


Fig. 4. UV-Vis absorption spectra of pure, ZnO:Cu, and ZnO:Mg nanoparticles.

stant, h is the Planck's constant, ν is the photon frequency, E_g is the energy band gap and n is 1/2 for a direct band gap semiconductor. An extrapolation of the linear region of a plot of $(\alpha h\nu)^{1/n}$ on the y-axis versus photon energy ($h\nu$) on the x-axis gives the value of the energy band gap.

In the case of copper doping, the results reveal that the dopant incorporation leads to decrease of band gap to 2.6 eV. This results are consistent with the reports of others. Since 3d orbital of Cu atom is much shallower than 3d orbital of Zn, when a Cu atom substitutes Zn in ZnO crystalline lattice, two effects are predictable: (1) strong coupling occurs between d orbital of Cu atom and p orbital of O atom, which narrows the direct band gap and (2) Cu 3d orbital creates impurity bands above the ZnO valance band [17].

Band gap studies also show that with Mg doping, optical band gap increases from 3.44 eV to 3.83 eV. This may be attributed to the fact that new defects are introduced after Mg atoms substitute Zn atoms and enter into ZnO lattice due to the electronegativity and ionic radius differences between Zn and Mg. Moreover, there are more electrons contributed by Mg dopant due to lower electron affinity of MgO compared to ZnO, which takes up the energy levels located in the bottom of the conduction band. As a result, the valence electrons require extra energy to be excited to higher energy states in the conduction band [18].

3.5. Antibacterial activity

Fig. 5 shows the growth curves of the nanofluids together with the negative control (pure bacterial culture without the addition of nanoparticles). As the value of the optical density (OD) at 600 nm represents the absorbance of the bacteria, therefore, an increase in the number of bacteria implies more light being absorbed by them. It can be seen that copper doping improves the antibacterial activity of the nanoparticles, whereas, Mg dopant decreases the bactericidal effect of the samples. It must be noted that these differences are significant, since according to McFarland standard, the absorption of 0.2 for *E. coli* bacteria is approximately equivalent to bacterial cell population of 3×10^8 .

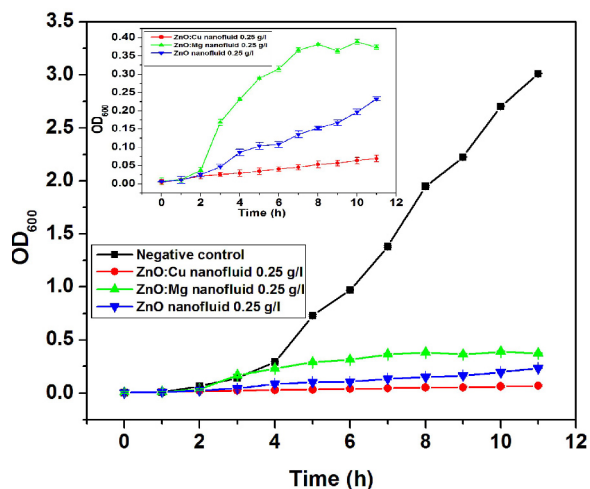


Fig. 5. Growth curve of *E. coli* in the presence of pure and doped ZnO nanoparticles, inset: the same plot in the OD range of 0 – 0.4 (negative plot curve is not plotted).

The higher bactericidal activity of ZnO:Cu samples could be due to reduction of particles' size and as a result, the increase in surface to volume ratio. Decrease of the band gap can also be a justifying reason. Band gap reduction and therefore possibility of exciton generation by visible light may lead to increased contribution of the photocatalyst mechanisms in bactericidal activity of Cu-doped samples whereas for ZnO:Mg nanoparticles, because of the increase in particles' size and energy band gap, a weaker antibacterial activity was observed.

4. Conclusions

Pure and Mg/Cu doped nanoparticles of ZnO were successfully synthesized via sol-gel method. According to structural studies, all samples were polycrystalline and had hexagonal wurtzite structure. The secondary phase of CuO monoclinic phase was observed in Cu doped sample. TEM images verified the growth of nanoparticles with relatively uniform size distribution. The average size of ZnO samples decreased with Cu incorporation while, addition of Mg increased the particles size. Optical studies revealed that Mg doping increases band gap while Cu doping resulted in decrease of the band gap. The antibacterial activities of the nanoparticles were tested against *Escherichia coli* cultures. Pure and doped ZnO nanofluids showed good antibacterial activity which increases with copper doping, and slightly decreased with addition of Mg.

References

- [1] ÖZGÜR Ü., ALIVOV Y.I., LIU C., TEKE A., RESHCHIKOV M.A., DOĞAN S., AVRUTIN V., CHO S.J., MORKOÇ H., *J. Appl. Phys.*, 98 (2005), 316.
- [2] ADJURIŠIĆ A.B., NG A.M.C., CHEN X.Y., *Prog. Quant. Electron.*, 34 (2010), 191.
- [3] WU C.C., WUU D.S., LIN P.R., CHEN T.N., HORNG R.H., *Nanoscale Res. Lett.*, 4 (2009), 377.
- [4] LIN L., FUJI M., WATANABE H., SHIRAI T., TAKAHASHI M., *Annu. Rep. ACRC*, 8 (2008) 17.
- [5] ÖZTAS M., BEDİR M., *Thin Solid Films*, 516 (2008), 1703.
- [6] OHIRA T., YAMAMOTO O., IIDA Y., NAKAGAWA Z., *J. Mater. Sci.-Mater. M.*, 19 (2008), 1407.
- [7] STOIMENOV P.K., KLINGER R.L., MARCHIN G.L., KLABUNDE K.J., *Langmuir*, 18 (2002), 6679.
- [8] ZHANG L., JIANG Y., DING Y., POVEY M., YORK D., *J. Nanopart. Res.*, 9 (2007), 479.
- [9] BRAYNER R., FERRARI-ILIOU R., BRIVOIS N., DJEDIAT S., BENEDETTI M.F., FIÉVE F., *Nano. Lett.*, 6 (2006), 866.
- [10] YAMAMOTO O., KOMATSU M., SAWAI J., NAKAGAWA Z., *J. Mater. Sci.-Mater. M.*, 15 (2004), 847.
- [11] YAMAMOTO O., SHIMURA T., SAWAI J., KOJIMA H., SASAMOTO T., *J. Ceram. Soc. Jap.*, 108 (2000), 156.
- [12] FERNANDES D.M., SILVA R., WINKLER HECHENLEITNER A.A., RADOVANOVIC E., CUSTÓDIO MELO M.A., GÓMEZ PINEDA E.A., "Synthesis and characterization of ZnO, CuO and a mixed Zn and Cu oxide", *Mater. Chem. Phys.*, 115 (2009), 110.
- [13] BIAN J., LOU Y., SUN J., LIANG H., LIU W., *J. Mater. Process. Tech.*, 189 (2007), 473.

-
- [14] GAYEN R.N., DAS S.N., DALUI S., BHAR R., PAL A.K., *J. Cryst. Growth*, 310 (2008), 4073.
- [15] SAHAR M.D.R., BUDI A.S., *J. Solid State Sci. Technol.*, 14 (2006), 115.
- [16] SONAWANE B.K., BHOLE M.P., PATIL D.S., *Physica B*, 405 (2010), 1603.
- [17] AHN K.S., DEUTSCH T., YAN Y., JIANG C., PERKINS C.L., TURNER J., AL-JASSIM M., *J. Appl. Phys.*, 102 (2007), 2.
- [18] CHEN H., DING J., MA S.H., *Physica E*, 42 (2010), 1487.

Received 2012-10-15
Accepted 2014-03-03